Dynamics of deuterium retention and desorption from plasma-facing materials in fusion reactor-relevant conditions

T. Sizyuk¹, T. Abrams²

¹Argonne National Laboratory, Lemont IL, USA ²General Atomics, San Diego CA, USA

Abstract

Hydrogen isotopes retention and desorption during and after discharges in fusion devices are still not well understood due to the complex device conditions and limitations of in-situ diagnostics and measurements. We simulated well-diagnosed recent experiments at the DIII-D facility to benchmark our ITMC-DYN integrated package of modeling deuterium diffusion, retention, and desorption during and after D discharge irradiation. Modeling results were compared with detail experimental data of D desorption fluxes for various irradiation conditions. We predicted the temporal evolution of free and trapped D distribution in tungsten (W) plasma-facing material (PFM). Effects of key parameters namely diffusion coefficient, recombination rate, trapping energies against different defect types, were examined in these simulations. Existing experimental data of these parameters in literature varies significantly which makes it harder to identify key mechanisms and physics responsible for hydrogen isotope retention and desorption. The purpose of this work is to accurately simulate recent well-diagnosed reactor experiments given the uncertainties in such parameters and identify mechanisms responsible for the retention and desorption. We implemented the best identified diffusion, recombination, and trapping parameters in ITMC-DYN package that integrate both various collisional and thermal processes. We predicted, for example, that sample cooling between discharges in DIII-D operations can significantly affect the spatial distribution of trapped D in W under reactor irradiation conditions. Correct prediction of desorption spectra from samples irradiated during 10 DIII-D discharges showed that up to 35% of D can be retained in high binding energy defects such as vacancy clusters or voids.

1. Introduction

The ability of plasma-facing materials (PFMs) in a fusion environment to withstand erosion during transient plasma events and damage/degradation during normal operation critically depends, among other factors, on the dynamics of deuterium and tritium retention and desorption

that can lead, e.g., to blistering and blisters bursting on the metallic surfaces [1]. Materials properties and composition will continuously be changing due to both collisional and thermal processes on the surface and sub-surface layers. Analysis of hydrogen isotopes transport and accumulation and the effects on PFMs in ITER-like and future fusion reactors requires further reactor-relevant experimental and advanced computer simulation analysis, including multi-physics integration, models validation, self-consistent simulations, and benchmarking to understand the integrated effects and the complex interplay of all the physical processes involved.

Critical areas of research on materials response to fusion plasmas include hydrogen isotopes implantation, recycling, retention, and related material degradation, e.g., in tungsten [2]; nanostructures formed by helium on the surfaces of metallic walls [3]; chemistry of isotopes uptake, e.g., in liquid PFMs [4-6]; neutron irradiation effects on resulting isotopes retention, e.g., in tungsten [7, 8]; transient plasma effects on material degradation [9]; melt layer erosion [10]; and irradiation of surrounding surfaces, e.g., for the ITER design [11]. Various materials and alloys used for the reactor walls and components can lead to significant amount of impurity redepositions on the divertor plate and on the walls. The evolving mixed materials will further change the dynamics of D and T deposition and co-deposition, desorption, and accumulation on the mixed surfaces and in the bulk. Self-consistent simulations implementing and integrating all relevant processes and effects, and numerical and experimental validation are required for accurate assessment of PFMs erosion lifetime performance as well as fuel retention in current and future fusion devices.

One of the important aspects, which calls for extensive models development and validation, is the simulation of the entire cycle of hydrogen isotopes retention/desorption during and between discharges in realistic reactor environments. Current modeling approaches for the analysis of D/T behavior in materials are mainly based on molecular dynamics (MD) and Monte Carlo (MC) simulations, rate equations-based models, and various combinations and integrations of the above methods. Due to the limitations of MD simulations, MC modeling of collisional processes integrated with deterministic rate equations is the most appropriate approach to simulate actual experimental conditions and set up, e.g., taking into account the time durations between the experiments and the diagnostics.

Combination of the rate and diffusion equations is a common approach for modeling hydrogen diffusion, trapping, and desorption in materials. There are several assumptions and uncertainties in the calculation of trapping and detrapping rates in these equations [12]. Jump frequency analysis based on the diffusion coefficient and lattice constant is most often used to calculate the rate of D trapping [13-15]. Trapping rates described by the Arrhenius law were used in previous work [16], where the pre-exponential factor is calculated from lattice vibration frequency and lattice constant, and the knowledge of the trapping activation energies is required. Several variations were also used in the calculation of D detrapping rate based on the Arrhenius representation, e.g., using the lattice vibration frequency [13,14,16] and the jump frequency calculated from the diffusion coefficient and lattice constant [15].

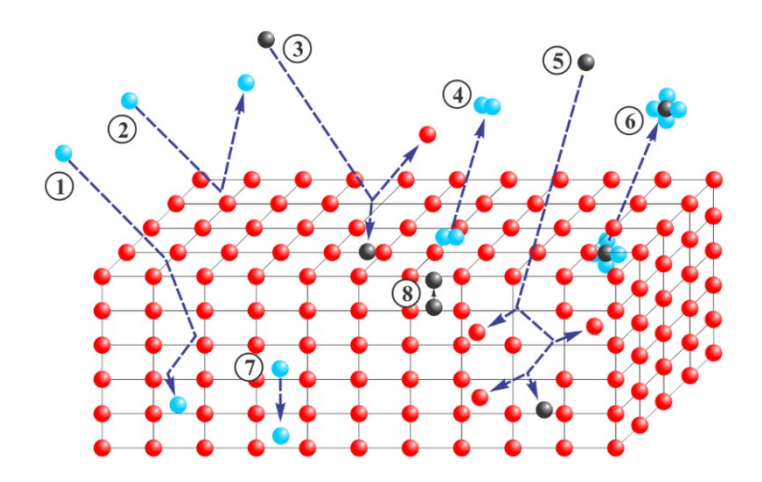
A challenging task to the solution of the above equations is the precise knowledge of key parameters which can be obtained from the experiments, or by ab-initio and classical MD and DFT calculations. However, the values obtained from different sources can vary significantly depending on the experimental conditions and/or the existing uncertainties in calculations, e.g., the interatomic potential.

In this work, we thoroughly examine several of the most important parameters, such as diffusion coefficient, recombination rate, trapping energies for different existing defects, and how these parameters affect the accuracy of the results as well as on the controlling physics of hydrogen isotope behavior in PFMs. We enhanced our ITMC-DYN package for the simulation of D interaction with materials during and after irradiation and implemented potential trapping sites retention as a function of the free (not trapped) D concentration and time. We performed detailed simulations based on recent experiments in the DIII-D tokamak machine. The above-mentioned key parameters were predicted in the simulations to reproduce the well-diagnosed experimental results.

2. Brief review of implemented models

We used our enhanced ITMC-DYN package that uniquely integrates all collisional and thermal processes relevant to plasma/material interactions in fusion reactors [17-20]. This package includes interatomic potential functions for detailed modeling of ion/atom collisions; models for energy loss of elastic and inelastic collisions; particles thermal diffusion and segregation processes near-surface layers, hydrogen isotope trapping, molecular surface recombination and desorption,

chemical and physical erosion, and calculation of rate coefficients in multi-component materials based on the dynamic material composition. The collisional processes responsible for target atoms sputtering, mixing, and particles reflection are therefore integrated with detailed models for temperature-dependent processes leading to temporal and spatial material evolution. All models are integrated in a self-consistent manner that allows accurate simulation of realistic experimental conditions and parameters, such as: multiple and simultaneous ions composition, energies, and fluxes; material characteristics and temperature; and the experimental setup. Figure 1 shows various interaction processes implemented in the package. The integrated models were extensively benchmarked with both in-house experiments and worldwide published data. As a result, the ITMC-DYN simulations explained several experimental data showing the importance of self-consistent time-dependent integration of the implemented models, e.g. [19]. The ITMC-DYN package is continuously being upgraded and enhanced for the analysis of PFMs in fusion reactor environments.



- (1) Scattering and trapping
- (2) Backscattering
- (3) Sputtering
- (4) Recombination and desorption
- (5) Cascade collision & displacement
- (6) Chemical reaction & erosion
- (7) Diffusion
- (8) Surface segregation

Dynamic D trapping sites accumulation as function of D concentration and time

Fig. 1. Various collisional and thermal processes integrated in ITMC-DYN simulation package.

The following set of deterministic rate equations is implemented and solved in ITMC-DYN Monte Carlo code to simulate deuterium diffusion, trapping, and desorption:

$$\frac{\partial C}{\partial t} = D \frac{\partial^2 C}{\partial z^2} - \sum_i \frac{\partial C_i}{\partial t} \tag{1}$$

$$\frac{\partial C_i}{\partial t} = \frac{D}{\lambda^2} C \frac{C_i^{tr} - C_i}{W} - C_i v \exp\left(-\frac{E_i}{kT}\right)$$

where: C is the concentration of deuterium in solution; C_i is the concentration of hydrogen trapped in the defect type i; W is the concentration of tungsten; D is the diffusion coefficient; C_i^{tr} is the concentration of traps; λ is the lattice constant ($\sim 3 \times 10^{-10}$ m); ν is the lattice vibration frequency (the Debye frequency, $\sim 10^{13}$ s⁻¹); E_i is the detrapping energy of defect type i; k is the Boltzmann constant; T is the temperature. The Gauss-Seidel method was used to solve the above system of equations. The adopted nonuniform mesh facilitated the solution of these equations for a large computational domain and the simulation of long durations of experiments and diagnostics with complex conditions.

The surface boundary conditions are represented by the desorbing flux of molecular deuterium (D₂) calculated based on the molecular recombination rate constant. We benchmarked various pre-exponential factors in the following equations to predict and explain the actual mechanisms and physics leading to the experimental results.

$$D = D_0 \exp\left(-\frac{E_d}{kT}\right) \qquad K = K_0 \exp\left(-\frac{E_r}{kT}\right) \tag{2}$$

where: *K* is the recombination rate, D₀ and K₀ are the pre-exponential factors for diffusion and recombination rates respectively, E_d and E_r are the activation energies for diffusion and recombination respectively. The Arrhenius forms of diffusion and desorption rates are used with activation energies of 0.39 eV [21] and about 1.16 eV [22] for D diffusivity and recombination in W, respectively. The activation energy for the recombination rate in [22] was obtained based on the permeation experiments and represents the average value of calculations for different, unannealed and annealed, samples. It was also assumed in these experiments that most of the initially found O and C impurities on the surface were removed during the first minute of irradiation by the 3 keV D³⁺ ions. This indicates that the results obtained are for a clean surface.

Our simulation of D trapping takes into account the concentration of the initial trapping sites in material and trapping sites agglomeration (e.g., multiple D trapping in vacancy) or agglomeration due to deuterium irradiation (e.g., vacancy clusters or voids growth). For these purposes, we implemented models for the trapping sites accumulation to predict temporal and

spatial evolution of D in these traps. Various experimental results showed that the spatial distribution of trapped D depends on, among other things, D flux, fluence, and material temperature [23, 24]. During irradiation, these parameters determine the temporal and spatial evolution of free D concentration which, in turn, determines the probability of D trapping, e.g., in vacancies and dislocations loops. We take this into account in our calculations of D trapping in existing defects. In addition, several recent DFT-based studies showed that hydrogen at interstitial sites can significantly reduce vacancy formation energy in W and increasing the number of surrounding hydrogen atoms further reduces this energy [25, 26]. The high supersaturation of D can also lead to supersaturation of vacancies that can results in vacancy clusters and void growth [27]. From this consideration the calculation of trapping sites accumulation, that is D trapping dynamics due to D supersaturation and various defects growth, is implemented in our model as a function of free D concentration and precalculated trapping rate using a semiempirical equation:

$$C_i^{tr} = C_i^{tr} + C_s * rate * \Delta t \tag{3}$$

where the rate is estimated based on the simulated experimental data as: rate $\approx \frac{D_{trapped}^{total}}{C_s*\Delta x_s*t}$, with $D_{trapped}^{total}$ corresponding to the measured trapped D fluence, C_s corresponding to the average concentration of free D on the surface predicted by ITMC-DYN simulation of the corresponding experimental setup, Δx_s is the thickness of surface layer, and t is the duration of the irradiation experiment. The surface layer is determined as a layer within which free D concentration does not vary significantly during irradiation time. The thickness of this layer depends on ion flux, fluence, and material temperature. D trapping rate in our model varies depending on trap types.

The semiempirical formula given in eq. 3 is therefore used to predict, based on the experimental data, the D trapped in various trapping sites in ITMC-DYN simulation. Introducing the trapping rate calculation and correlation of this rate with free D concentration is the major difference between our model and other models where similar rate equations are used. This new approach helps then to explain the difference in spatial distribution of trapped D. Finding the general dependencies of D trapping rate on various irradiation conditions will lead to the development of predictive modeling of hydrogen isotopes accumulation in PFMs.

3. Simulation results and discussions

3.1. Evaluation of deuterium diffusion and desorption rates

The interplay between the two main processes, diffusion and desorption through molecular recombination on the surface, determines the dynamics of hydrogen isotopes accumulation in tungsten. There are many uncertainties in these parameters and their temperature dependences arising from the differences between different experimental setups, accuracy of diagnostics, and calculation methodology [28]. Various DFT calculations showed large variations in the predicted diffusion coefficients, especially at low temperatures [29-31]. Recent DFT-based work [30] showed that two regimes should be considered in the calculation of hydrogen diffusivity: the first regime is determined by the diffusion of interstitial hydrogen from one tetrahedral site to another; the second regime is determined by D diffusion between vacancies and occurs at lower temperatures. This work proposed also that the activation energy for D diffusion in low temperature regime can be related to D de-trapping energy that results in two-three times higher activation energy than the commonly used 0.39 eV. Another study, based on experimental data, correlated deuterium diffusivity to the trapping energies of D in tungsten [32]. MD simulations showed significant reduction in the diffusion coefficient with increasing of hydrogen concentration in tungsten [33].

The measurement and correct prediction of the diffusion and recombination coefficients can have strong dependence on the experimental setup and irradiation conditions. We used recent experiments at DIII-D to predict these parameters as well as for the analysis of D trapping in fusion reactor conditions [34]. Various diagnostics were used in these experiments to measure particle and heat flux to the surface, temporal evolution of samples temperature during and in between discharges. Spatial distribution of trapped D after 10 discharges was measured by NRA; total retained D was detected by TDS technique heating the sample with 0.5 K/s rate. We simulated the process of W irradiation by D ions using the predicted 100 eV ion energy and the measured flux during the discharges and varying the temperature of the samples according to the measurement. We also simulated D diffusion and desorption between discharges.

Initially, we modeled diffusion and desorption processes without trapping effects to predict an effective diffusion coefficient for these samples. The presence of C impurities in the DIII-D tokamak, up to 1-2%, and resulting W surface contamination [35, 36] can significantly affect D

transport on the surface and retention in PFMs. The dependence on D diffusivity was analyzed using a fixed activation energy of 0.39 eV and varying the pre-exponential factor D₀. Figures 2 show NRA data and the simulation results for pristine ITER grade W: a) spatial D distribution at the end of discharge when sample was heated to the high temperature of 470K and b) spatial D distribution between discharges when the sample was cooled to the low temperature of 330K. Figures 2 show simulation results of spatial distribution of total D during and after the first discharge in multi-pulsed operation.

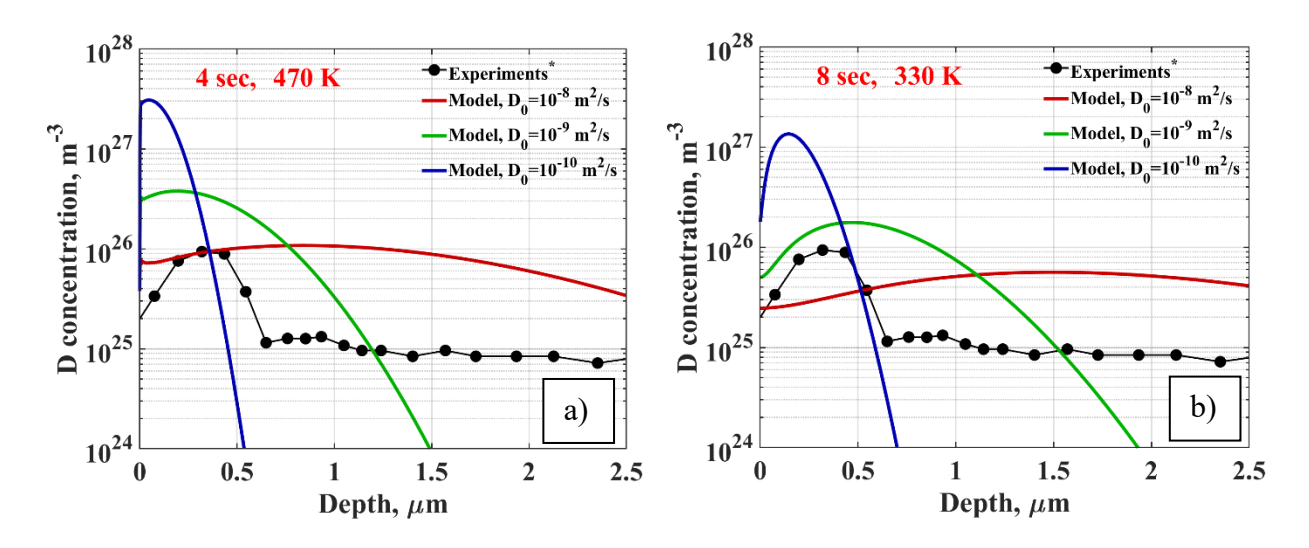


Fig. 2. D spatial distribution (a) during and (b) between discharges predicted with various diffusion coefficients (varying pre-exponential factor). Experimental data show NRA measurements for pristine ITER grade W after 10 discharges in DIII-D [34].

NRA data showed an order of magnitude higher trapped D concentration at 0.3-0.4 µm from the surface (Fig. 2). Assuming uniform initial defects and impurities distribution in the pristine sample, this large gradient in the spatial concentration of trapped D can only be explained by the difference in initially free D distribution during and after irradiation. From this consideration, we can predict that the effective diffusion coefficient for these sample can be calculated with the pre-exponential factor in the range between 10⁻⁹ m²/s and 10⁻¹⁰ m²/s. While the highest concentration of free D during irradiation is near the surface, the measured concentration of trapped D on the surface is five times lower than at the peak location. This can be explained by higher temperatures (100-150K higher) in the samples during the irradiation compared to the cooling period that results in much higher D solubility and diffusivity preventing D trapping and traps agglomeration around this location.

To further analyze D diffusivity and desorption rates for samples irradiated at DIII-D, we simulated D desorption flux as a function of temperature during samples heating relevant to TDS measurements. First, we simulated the desorption spectra from the ultra-fine grain (UFG) W sample pre-irradiated by 12 MeV Si ions that produced up to 0.6 dpa. The trapped D spatial distribution obtained from NRA measurements was used for the simulation of D desorption during sample heating with 0.5 K/s rate. In this sample 100% of D was accumulated within the measured thickness of 3.5 μm from NRA [34]. The majority of the retained D was assumed to be in low energy trapping sites. Figure 3 shows the results of simulations and the effect of the diffusion coefficient on D desorption flux and comparison with TDS measurements. Our simulations predicted mean de-trapping energies for this sample as ~0.9 eV corresponding to the peak at around 470 K temperature and higher de-trapping energies as ~2.15 eV and ~2.5 eV corresponding to the temperature range from 800 K to 1200 K.

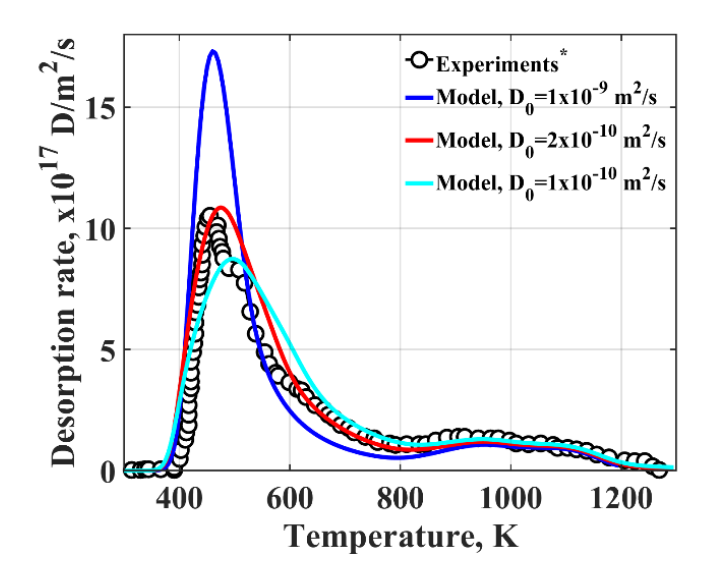
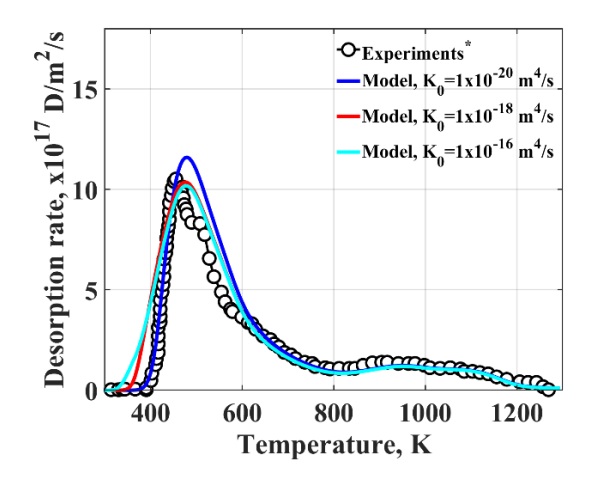


Fig. 3. Effect of diffusion coefficient on D desorption spectrum from W sample pre-irradiated by Si ions up to 0.6 dpa and exposed to plasma during 10 pulses in DIII-D machine. Experimental data is from [34].

A diffusion coefficient with the preexponential factor of 1-2 x 10⁻¹⁰ m²/s range in the low temperature regime is justified for W in this case. The desorption spectra in these simulations are influenced by both the diffusion coefficient and by the de-trapping energies, while no significant effect of the recombination coefficient was found. Figure 4 shows the dependence of desorption spectrum on various recombination rates calculated using a fixed activation energy of 1.16 eV and

varying the pre-exponential factor K₀. The small effect of the desorption rate can be explained by the relatively low diffusion coefficient at low temperatures that can be characterized as a diffusion limited regime. With increasing sample temperature, D desorption is mainly determined by the dynamics of D de-trapping from high-energy traps.



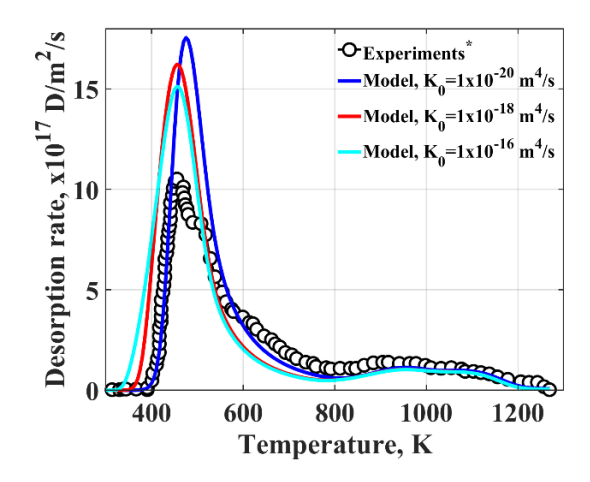


Fig. 4. Effect of recombination coefficient on D desorption spectrum from damages UFG W sample. Two sets of diffusion coefficients were used: $D_0 = 2x 10^{-10} \text{ m}^2/\text{s}$ (left) and $D_0 = 10^{-9} \text{ m}^2/\text{s}$ (right). Experimental data is from [34].

We correlated the predicted de-trapping energies with the possible defects in the samples based on the review of DFT works and experimental data. Many DFT based calculations predicted energies of hydrogen isotopes de-trapping from W vacancies [25,29,30,37,38]. However, the range of the predicted energies of a single trapped in vacancy hydrogen atom vary from 0.73 eV (considering only de-trapping from vacancy to interstitial position) to 1.79 eV that cause significant uncertainties in this important parameter. Therefore, association of de-trapping energies with various traps was estimated in our analysis based on the average predicted DFT results and based on the experimental data.

The average dpa produced by Si ions near sample surfaces was around 0.15 dpa [34]. Even taking into account that most of interstitial and vacancies recombine after Si ion irradiation, there are still significant number of vacancies in the damaged or irradiated area. These vacancies serve as the main trapping centers for deuterium. The average de-trapping energy corresponding to 470K temperature peak is around 0.9 eV. According to several DFT based studies, this energy can correspond to de-trapping of multiple trapped D in single vacancy or dislocation, e.g., this average energy was predicted for 6-7 [30,37] D atoms trapped in a single vacancy or ~3 D atoms trapped

in a dislocation [39]. The majority of the retained D in this sample was in low, 0.9 eV, energy traps indicating that most vacancies in pre-damaged UFG W samples irradiated by plasma at relatively low temperatures are preferentially occupied by multiple D atoms. From this, we can determine the filled vacancy concentration in the pre-damaged area as $\sim 0.06\%$.

A small amount, about 10%, of D is trapped in the defects produced and/or agglomerated during the irradiation that is related to the slight increase in the desorption spectra at 800K-1200K (Fig. 4). Corresponding 2.15 eV - 2.5 eV de-trapping energies can be associated with large vacancy clusters or voids [40, 41]. These defects can be attributed, for example, to the growth of nanovoids leading to higher average D binding energies in these defects. According to the results of extensive experiments on hydrogen-defect interactions, D release at 630 K temperature may correspond to D accumulation in small, 20 nm, voids [42] but more detail data and analysis are required. These experiments suggested also that D release at 750K temperature corresponds to D accumulation in small vacancy clusters which could be produced during annealing processes or during the irradiation, e.g., due to hydrogen supersaturation. Nanovoids can exist in samples annealed prior to irradiation [42] or can be created by D precipitation [43,44]. Other studies predicted hydrogen bubble nucleation and growth from vacancies when a critical H concentration is reached [45]. Accumulation of D in damaged UFG W at relatively low (~430K) irradiation temperature could then be described by two processes: preferentially multiple trapped D in a single vacancy and/or dislocation and D trapping in vacancy clusters and voids with the growth of these defects.

3.2 D retention at elevated temperatures during pulsed operation

The above analysis showed that deuterium retention in pre-damaged W at relatively low temperatures for the considered fluences [34] is mostly determined by filling of vacancies with multiple D atoms per vacancy. In pristine tungsten, D retention in vacancies is limited due to the smaller amount of these defects. We simulated D desorption from another sample, high purity (ITER grade) W, recently studied in DIII-D. The undamaged ITER-grade W was irradiated at similar discharge conditions, however the measured temperature on the surface was higher during the irradiation and varied from 330K up to 470K. Only 25% of the retained D accumulated within 3.5 μm of the surface [34]. We used D spatial concentrations from NRA measurements within this layer and assumed uniform D distribution up to 40 μm with around 10⁻⁴ atomic concentration that is similar to the concentration measured at the 3.5 μm location. We also assumed that high energy

traps (2.1eV - 2.5 eV), which are usually produced in samples irradiated at high temperatures, are located only within the first \sim 8.5 μ m that corresponds to the maximum range where substantial amount of D diffuses during 10 pulses of operation. Figure 5 shows the simulation results of D desorption spectra from this sample and comparison with the DIII-D experimental data.

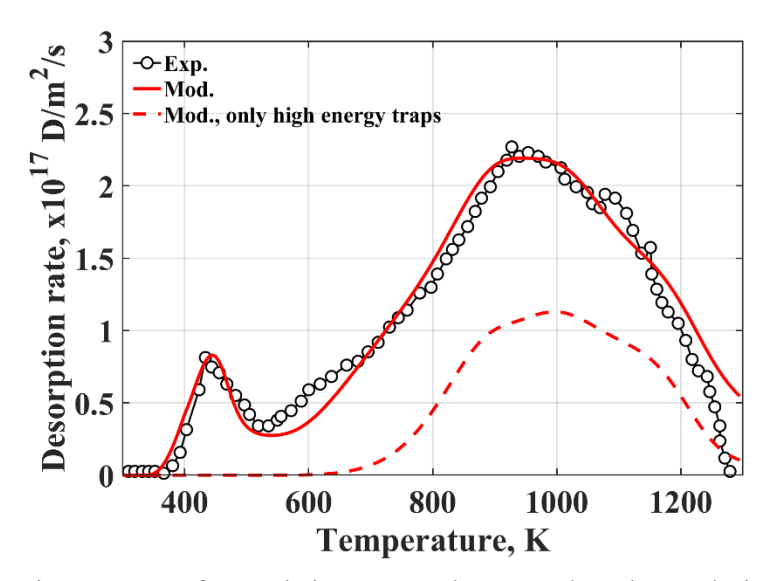


Fig. 5. D desorption spectrum from pristine W sample exposed to plasma during 10 discharges in DIII-D machine. Experimental data is from [34].

These simulations showed that about 35% of D is accumulated in high energy traps. Significant contribution to the desorption flux at high temperatures is de-trapped D from the low energy trapping sites, around 1 eV, located deep in the bulk. This is illustrated in Fig. 5 where the portion of D desorbed from high energy traps is shown by dash line. Simultaneous D trapping/de-trapping due to the relatively high concentration of D released from the traps and limited diffusivity to the surface will result in delayed desorption of D released from low energy traps located far from the surface. Deuterium can be accumulated in low energy intrinsic traps in the bulk after irradiation when material is cooled down and the free D concentration is lower than the limit for high energy traps formation/accumulation.

The first peak in the desorption spectrum shown in Fig. 5 corresponds to the peak in D spatial distribution located at \sim 0.2-0.5 μm from the surface obtained from NRA measurements. We predicted the mechanism of this peak formation in the case of undamaged W sample where uniform defects distribution is assumed. We simulated D irradiation of W sample during the discharge and D diffusion and desorption between discharges with an average $1.75 \times 10^{22} \, D^+/m^2/s$

ion flux and 100 eV energy. The duration of each discharge was 4 sec and the time between discharges was 15 minutes. Temperature changes during each discharge and between discharges were measured and we used the same temperature evolution in our simulations [34]. We assumed about 10^{-4} concentration of intrinsic traps in these simulations. Figure 6 shows the spatial distribution of free and trapped D at the beginning of the first discharge and 1 min after when the sample temperature was cooled down to 330K. These results were obtained using $D_0 = 2x10^{-10}$ m²/s and $K_0 = 10^{-16}$ m⁴/s.

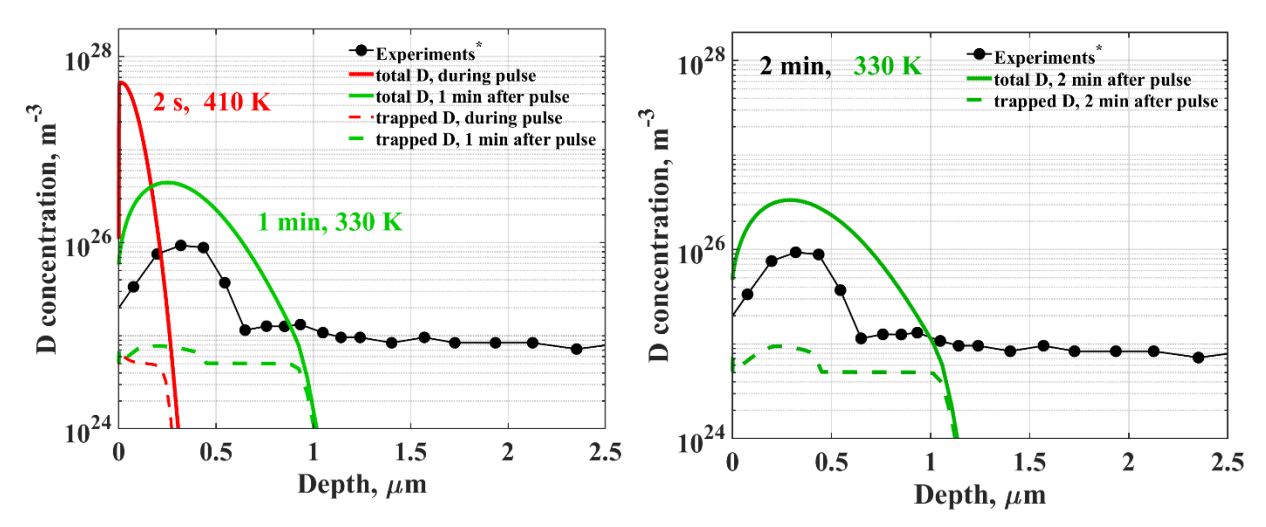


Fig. 6. Free and trapped D spatial distribution during and after first pulse of DIII-D discharge. Experimental data is from [34].

Fig. 7. Dynamics of D trapping during the cooling between discharges. Experimental data is from [34].

It is clear from Fig. 6 that the dynamics of sample cooling determines the location of the D concentration peak. Low temperature leads to decreasing both the diffusivity and solubility, and together with the relatively high D concentration at the peak location results in enhanced D trapping in existing defects and defects formation and agglomeration. Figure 7 shows D trapping behavior during the cooling process. The trapping sites accumulation was calculated using the Eq. 3. The very short time (4 sec) when free D concentration is high at the surface during the discharge and due to the following desorption and diffusion in the bulk explains the relatively low concentration of trapped D near the surface. Figure 8 shows simulation results of free and trapped D distribution at several days after irradiation and comparison with NRA measurements.

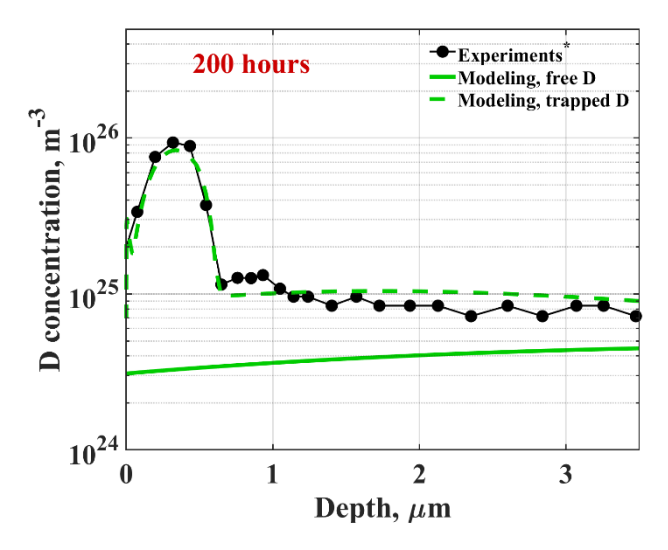


Fig. 8. Trapped and free D distribution 200 hours after irradiation predicted in simulations and comparison with NRA profile. Experimental data is from [34].

An order of magnitude more D is accumulated at ~0.2-0.5 µm from the surface in both low and high energy traps compared to surrounding areas. As a result, we can conclude that low energy traps, vacancies or dislocations, were produced or D₂ molecules were accumulated in voids in this area as well. Several studies showed that hydrogen interstitial reduces vacancy formation energy in W and increasing hydrogen concentration significantly enhances this effect [25,46]. Reducing vacancy formation energy was explained by the changing in the charge distribution of W atom induced by multiple H [46], especially in the presence of impurities [47]. The reduction in vacancy formation energy was also explained by hydrogen association with self-interstitial clusters [48]. On the other hand, experimental studies showed that 1 eV -1.4 eV energies can correspond to the release of hydrogen molecule from voids [40].

3.3 Effect of irradiation temperature on D trapping in low and high binding energy defects

We studied the effect of irradiation temperature on preferential D retention in low and high energy traps in pre-damaged ITER grade W samples irradiated at different temperatures. Figure 9 shows twice more trapped D was detected in sample irradiated at 90K higher temperature (i.e., 530K vs. 440K). ITMC-DYN simulation results perfectly matched the well diagnosed experimental data of DIII-D. Simulation of D desorption flux as a function of temperature during samples heating and comparison with TDS data predicted trapped D distribution in different defects determined from de-trapping energies.

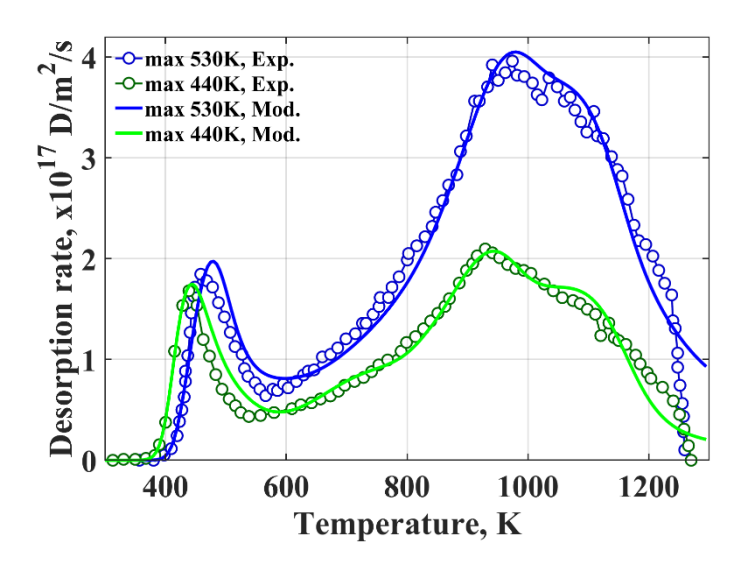


Fig. 9. D desorption spectra from ITER grade W pre-damaged with 0.6 dpa in dependence on maximum irradiation temperatures. Experimental data is from [34].

Modeling results predicted mean de-trapping energies as 0.95 eV for the low temperature sample and 1.05 eV for the higher temperature sample during the irradiation; corresponding to the first desorption peak at 450K and 480K temperatures in TDS spectra. The mean de-trapping energies corresponding to the second peak are similar for both samples, i.e., in the range of 2.15 eV to 2.55 eV. Twice more D is retained at the higher irradiation temperature of 530K. However, relative distribution of D in low- and high-energy traps are similar. The difference in the amount of retained D can be explained by the difference in D diffusion. Higher D diffusion in the sample irradiated at higher temperature along with relatively low desorption from the surface (due to presence of C impurities on surface) results in more D accumulated in bulk.

The above samples were pre-damaged by 12 MeV Si ions. Based on SRIM calculations, the depth of damage by Si ions was \sim 2.5 μ m with a peak at \sim 2 μ m. The experimental data showed that peak of trapped D does not correspond to this peak of damage. This can indicate as predicted in our modeling that D supersaturation at certain location can be the main mechanism for traps accumulation at this location in ITER grade W samples.

3.4 Effect of different damage on D trapping in low and high binding energy defects

We studied the effect of the damage rate (dpa) on the dynamics of D desorption and retention. The analysis of W damage effect on D trapping in different defects was done based on damaged UFG W samples irradiated at approximately similar temperatures. Figure 10 shows simulation results of D desorption spectra and comparison with TDS data.

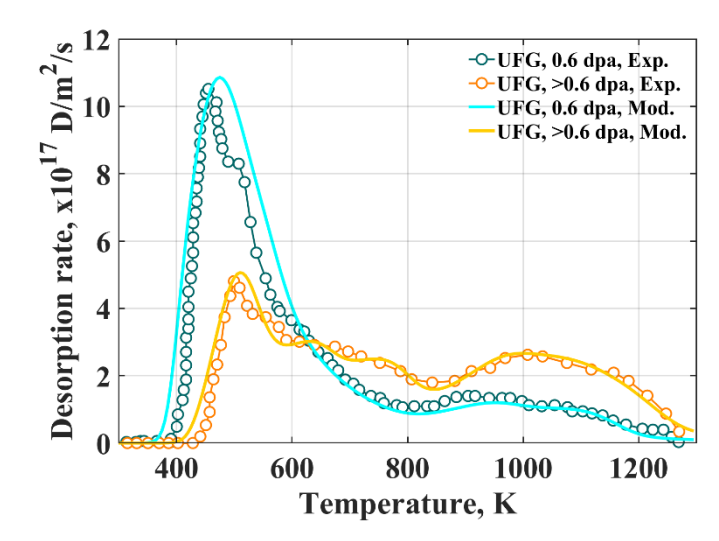


Fig. 10. D desorption spectra from UFG grade W at different damage. Experimental data is from [34].

The analysis of damaged UFG W samples showed that with roughly similar total retained D, much more D is retained in high energy traps in the case of higher dpa (>0.6 dpa). Significant fraction of the retained D in more damaged samples is in traps with 1.4 eV - 1.7 eV de-trapping energies that correspond to vacancy clusters/small voids [42]. Simulations showed that D retention in vacancy clusters is within ~2.5 μ m range that well corresponds to the range of damage produced by 12 MeV Si ions.

Recent simulations using the creation-relaxation algorithm (CRA) showed saturation of vacancies with increasing dpa due to equilibrium between the generation and annihilation of defects [49]. That is, increasing dpa does not usually increase number of vacancies but leads to vacancy clusters formation. The two UFG samples from DIII-D experiments at different damage rates illustrate the transition from preferential trapping in vacancies (0.6 dpa) to enhanced trapping in vacancy clusters and voids (>0.6 dpa). From this, one can conclude that increasing dpa leads to D retention in higher energy traps explained by more vacancy clusters formation that results in voids production and growth.

4. Conclusion

We have developed and implemented a new dynamic approach for the simulation of hydrogen isotopes implantation, diffusion, trapping, and desorption. This new approach allowed successful reproduction of various DIII-D tokamak experimental results. Our enhanced models implemented in the ITMC-DYN simulation package predicted that the details and dynamics of sample cooling during the multi discharge operation determines the location of D concentration peak in the subsurface region. At elevated implantation temperatures, shifting of the D peak concentration from the surface during the cooling processes in between discharges and the decreased solubility and diffusivity at lower temperature leads to trapped D accumulation in the area around the peak location. Based on the simulation of D accumulation in vacancies/dislocations and in higher energy traps, we infer that the high concentration of vacancies in the damaged W delayed void growth compared with undamaged samples. However, increasing dpa leads to vacancy clusters formation and enhanced D retention in high energy traps.

Continues neutron produced damage in future large devices like ITER can lead to formation of high energy traps in W that can result in degradation and enhanced D/T retention. While larger reactors will operate at much longer pulses than DIII-D, the spatial and temporal variation in temperatures together with continuous neutron irradiation would lead to non-uniform distribution and accumulation of trapped isotopes in subsurface layers. However, both experiments and our simulations showed the significant effect of material properties on this process.

In this study we did not consider details of material structure. Grain boundaries can affect defects generation and migration that will be investigated in our future studies of irradiated samples. Overall, this new approach and results explained the importance of the interplay of D diffusion, desorption, and trapping sites accumulation in pristine and damaged samples in determining the correct physics driving hydrogen isotope behavior and retention in plasma facing materials in reactor environment.

Acknowledgments

This material is based upon work supported by the U.S. Department of Energy, Office of Science/Office of Fusion Energy Sciences, at Argonne National Laboratory under contract DE-AC02-06CH11357 and at the DIII-D National Fusion Facility under contract DEFC02-04ER54698.

Disclaimer: This report was prepared as an account of work sponsored by an agency of the United States Government. Neither the United States Government nor any agency thereof, nor any of their employees, makes any warranty, express or implied, or assumes any legal liability or responsibility for the accuracy, completeness, or usefulness of any information, apparatus, product, or process disclosed, or represents that its use would not infringe privately owned rights. Reference herein to any specific commercial product, process, or service by trade name, trademark, manufacturer, or otherwise does not necessarily constitute or imply its endorsement, recommendation, or favoring by the United States Government or any agency thereof. The views and opinions of authors expressed herein do not necessarily state or reflect those of the United States Government or any agency thereof.

References

- 1. W.M. Shu, E. Wakai and T. Yamanishi, Blister bursting and deuterium bursting release from tungsten exposed to high fluences of high flux and low energy deuterium plasma, Nucl. Fusion 47 (2007) 201–209.
- 2. T. Tanabe, Review of hydrogen retention in tungsten, Phys. Scr. T159 (2014) 014044.
- 3. S. Gonderman, J.K. Tripathi, G. Sinclair, T.J. Novakowski, T. Sizyuk and A. Hassanein, Effects of in situ dual ion beam (He+ and D+) irradiation with simultaneous pulsed heat loading on surface morphology evolution of tungsten–tantalum alloys, Nucl. Fusion 58 (2018) 026016.
- 4. P.S. Krstic, J.P. Allain, C.N. Taylor, J. Dadras, S. Maeda, K. Morokuma, J. Jakowski, A. Allouche, C.H. Skinner, Deuterium Uptake in Magnetic-Fusion Devices with Lithium-Conditioned Carbon Walls, Phys. Rev. Lett. 110 (2013) 105001.
- 5. J.P.S. Loureiro, H. Fernandes, F.L. Tabarés, G. Mazzitelli, C. Silva, R. Gomes, E. Alves, R. Mateus, T. Pereira, H. Figueiredo, H. Alves, Deuterium retention in tin (Sn) and lithium—tin (Li—Sn) samples exposed to ISTTOK plasmas, Nuclear Materials and Energy 12 (2017) 709.
- 6. T. W. Morgan, P. Rindt, G. G. van Eden, V. Kvon, M. A. Jaworksi and N. J. Lopes Cardozo, Liquid metals as a divertor plasma-facing material explored using the Pilot-PSI and Magnum-PSI linear devices, Plasma Phys. Control. Fusion 60 (2018) 014025.
- 7. M.H.J. 't Hoen, M. Mayer, A.W. Kleyn, H. Schut and P.A. Zeijlmans van Emmichoven, Reduced deuterium retention in self-damaged tungsten exposed to high-flux plasmas at high surface temperatures, Nucl. Fusion 53 (2013) 043003.
- 8. Y. Oya, et al, D retention and depth profile behavior for single crystal tungsten with high temperature neutron irradiation, Journal of Nuclear Materials 539 (2020) 152323.
- 9. A. Suslova, O. El-Atwani, D. Sagapuram, S. S. Harilal and A. Hassanein, Recrystallization and grain growth induced by ELMs-like transient heat loads in deformed tungsten samples, Scientific Reports 4 (2014) 6845.
- 10. G. Miloshevsky and A. Hassanein, Stability and erosion of melt layers developed on plasma facing components of tokamaks, Nucl. Fusion 54 (2014) 043016.
- 11. V. Sizyuk and A. Hassanein, Comprehensive 3-D simulation and performance of ITER plasma facing and nearby components during transient events Serious design issues, Phys. Plasmas 25 (2018) 062508.
- 12. A. Hu, Modeling Hydrogen Isotope Behavior in Fusion Plasma-Facing Components, (Doctoral dissertation). Retrieved from ProQuest Dissertations and Theses (2014).
- 13. M. I. Baskes, (Sandia National Laboratories. Report, SAND83-8231, 1983).

- 14. K. L. Wilson, R. Bastasz, R. A. Causey, D. K. Brice, B. L. Doyle, W. R. Wampler, W. Moller, B. M. U. Scherzer and T. Tanabe, Nuclear Fusion 1, 31-50 (1991).
- 15. O. V. Ogorodnikova, Fundamental aspects of deuterium retention in tungsten at high flux plasma exposure, Journal of Applied Physics 118, 074902 (2015).
- 16. J. Guterl, R.D. Smirnov, S.I. Krasheninnikov, M. Zibrov and A.A. Pisarev, Theoretical analysis of deuterium retention in tungsten plasma-facing components induced by various traps via thermal desorption spectroscopy, Nucl. Fusion 55 (2015) 093017.
- 17. A. Hassanein, Surface Effects on Sputtered Atoms and their Angular and Energy Dependence, Fusion Technology 8 (1985) 1735
- 18. T. Sizyuk and A. Hassanein, Dynamic analysis and evolution of mixed materials bombarded with multiple ions beams, Journal of Nuclear Materials 404, 60-67 (2010).
- 19. T. Sizyuk and A. Hassanein, Effect of surface segregation and mobility on erosion of plasma-facing materials in magnetic fusion systems, Journal of Nuclear Materials 458, 312 (2015).
- T. Sizyuk, A. Hassanein, Dynamic evolution of plasma facing surfaces in NSTX: impact of impurities and substrate structure on fuel recycling, Journal of Nuclear Materials 438, S1109-S1112 (2013).
- 21. R. Frauenfelder, Solution and Diffusion of Hydrogen in Tungsten, Journal of Vacuum Science and Technology 6 (1969) 388.
- 22. R. A. Anderl, D. F. Holland, G. R. Longhurst, R. J. Pawelko, C. L. Trybus, C. H. Sellers, Deuterium transport and trapping in polycrystalline tungsten, Fusion Technol. 21 (1992) 745.
- 23. V.Kh. Alimov, J. Roth, R.A. Causey, D.A. Komarov, Ch. Linsmeier, A. Wiltner, F. Kost, S. Lindig, Deuterium retention in tungsten exposed to low-energy, high-flux clean and carbon-seeded deuterium plasmas, Journal of Nuclear Materials 375 (2008) 192–201.
- 24. D. Nishijima, R.P. Doerner, M.J. Baldwin and G.R. Tynan, Dynamic deuterium retention properties of tungsten measured using laser-induced breakdown spectroscopy, Nucl. Fusion 61 (2021) 116028.
- 25. S.C. Middleburgh, R.E. Voskoboinikov, M.C. Guenette, D.P. Riley, Hydrogen induced vacancy formation in tungsten, Journal of Nuclear Materials 448 (2014) 270–275.
- 26. E. A. Hodille, N. Fernandez, Z. A. Piazza, M. Ajmalghan, and Y. Ferro, Hydrogen supersaturated layers in H/D plasma-loaded tungsten: A global model based on thermodynamics, kinetics and density functional theory data, Physical Review Materials 2, 093802 (2018).
- 27. J.B. Condon and T. Schober, Hydrogen bubbles in metals, Journal of Nuclear Materials 207 (1993) 1-24.
- 28. R. A. Causey, Hydrogen isotope retention and recycling in fusion reactor plasma-facing components, Journal of Nuclear Materials 300 (2002) 91–117.
- 29. D. F. Johnson and E. A. Carter, Hydrogen in tungsten: Absorption, diffusion, vacancy trapping, and decohesion, J. Mater. Res., Vol. 25 (2) (2010).
- 30. N. Fernandez, Y. Ferroa, and D. Kato, Hydrogen diffusion and vacancies formation in tungsten: Density Functional Theory calculations and statistical models, Acta Materialia 94 (2015) 307–318.

- 31. Anil Boda, Musharaf Ali Sk, K.T. Shenoy, Sadhana Mohan, Diffusion, permeation and solubility of hydrogen, deuterium and tritium in crystalline tungsten: First principles DFT simulations, International Journal of Hydrogen Energy 45, Issue 53 (2020) 29095.
- 32. J.L. Barton, Y.Q. Wang, R.P. Doerner and G.R. Tynan, Model development of plasma implanted hydrogenic diffusion and trapping in ion beam damaged tungsten, Nucl. Fusion 56 (2016) 106030.
- 33. T. Ahlgren, L. Bukonte, Concentration dependent hydrogen diffusion in tungsten, Journal of Nuclear Materials 479 (2016) 195-201.
- 34. J.L. Barton, D.A. Buchenauer, W.R. Wampler, D.L. Rudakov, Z.Z. Fang, C.J. Lasnier, J.A. Whaley, J.G. Watkins, E.A. Unterberg, R.D. Kolasinski, H.Y. Guo, Retention properties in displacement damaged ultra-fine grain tungsten exposed to divertor plasma, Nuclear Materials and Energy 20 (2019) 100689.
- 35. J.N. Brooks, T. Sizyuk, G. Sinclair and A. Hassanein, Tungsten–carbon surface evolution and erosion modeling for a small angle slot divertor in DIII-D, Nucl. Fusion 61 (2021) 126071.
- 36. J.N. Brooks, T. Sizyuk, J.D. Elder, T. Abrams, A. Hassanien, D.L. Rudakov, W. Wampler, Modeling, analysis, and code/data validation of DIII-D tokamak divertor experiments on ELM and non-ELM plasma tungsten sputtering erosion, Nucl. Fusion 60 (2020) 126026.
- 37. Kazuhito Ohsawa, Junya Goto, Masahiro Yamakami, Masatake Yamaguchi, and Masatoshi Yagi, Trapping of multiple hydrogen atoms in a tungsten monovacancy from first principles, Physical Review B 82, 184117 (2010).
- 38. K. Heinola, T. Ahlgren, K. Nordlund, and J. Keinonen, Hydrogen interaction with point defects in tungsten, Physical Review B 82, 094102 (2010).
- 39. W. Xiao, W.T. Geng, Role of grain boundary and dislocation loop in H blistering in W: A density functional theory assessment, Journal of Nuclear Materials 430 (2012) 132-136.
- 40. A. Van Veen, H. A. Filius, J. De Vries, K. R. Bijkerk, G. J. Rozing, and D. Segers, Hydrogen exchange with voids in tungsten observed with TDS and PA, J. Nucl. Mater., 155-157 (1988) 1113.
- 41. S. Ryabtsev, Yu. Gasparyan, M. Zibrov, A. Shubina, A. Pisarev, Deuterium thermal desorption from vacancy clusters in tungsten, Nuclear Instruments and Methods in Physics Research B 382 (2016) 101–104.
- 42. A. Rusinov, Yu. Gasparyan, N. Trifonov, A. Pisarev, S. Lindig, M. Sakamoto, Investigation of hydrogen-defect interaction in tungsten by the probe fluence method, Journal of Nuclear Materials 415 (2011) S645–S648.
- 43. W R Wampler and R P Doerner, Deuterium retention in tungsten from exposure to plasma, Phys. Scr. T138 (2009) 014037.
- 44. R.D. Kolasinski, D.F. Cowgill, D.C. Donovan, M. Shimada, and W.R. Wampler, Mechanisms of gas precipitation in plasma-exposed tungsten, J. Nucl. Mater. 438 (2013) S1019.
- 45. Lu Sun, Shuo Jin, Hong-Bo Zhou, Ying Zhang, Wenqing Zhang, Y Ueda, H T Lee and Guang-Hong Lu, Critical concentration for hydrogen bubble formation in metals, J. Phys.: Condens. Matter 26 (2014) 395402.

- 46. Shi-Yao Qin, Shuo Jin, Lu Sun, Hong-Bo Zhou, Ying Zhang, Guang-Hong Lu, Hydrogen assisted vacancy formation in tungsten: A first-principles investigation, Journal of Nuclear Materials 465 (2015) 135-141.
- 47. X.B. Ye and B.C. Pan, Interstitial hydrogen atoms in W-nitride compounds promoting the formation of atomic vacancies in nuclear fusion reactors, Nuclear Materials and Energy 32 (2022) 101229.
- 48. Yi-Nan Liu, T. Ahlgren, L. Bukonte, K. Nordlund, Xiaolin Shu, Yi Yu, Xiao-Chun Li, and Guang-Hong Lu, Mechanism of vacancy formation induced by hydrogen in tungsten, AIP Advances, 3, 122111 (2013).
- 49. A. Hollingsworth, et al., Comparative study of deuterium retention and vacancy content of self-ion irradiated tungsten, Journal of Nuclear Materials 558 (2022) 153373.